Available online at www.sciencedirect.com
SCIENCE DIRECT®
Earth and Planetary Science Letters 238 (2005) 311–328
EPSL
www.elsevier.com/locate/epsl

In situ X-ray diffraction study of post-spinel transformation in a peridotite mantle: Implication for the 660-km discontinuity

Konstantin Litasov [a,*], Eiji Ohtani [a], Asami Sano [a], Akio Suzuki [a], Kenichi Funakoshi [b]

[a] *Institute of Mineralogy, Petrology and Economic Geology, Faculty of Science, Tohoku University, Aoba-ku, Sendai 980-8578, Japan*
[b] *SPring-8, Japan Synchrotron Radiation Research Insitute, Kouto, Hyogo, 678-5198, Japan*

Received 6 January 2005; received in revised form 4 August 2005; accepted 4 August 2005
Available online 21 September 2005
Editor: R.D. van der Hilst

Abstract

We present the phase relations in anhydrous CaO–MgO–FeO–Al_2O_3–SiO_2–pyrolite to examine the influence of compositional difference between pyrolite and Mg_2SiO_4 on the post-spinel phase transformation. It is shown that in the pyrolite system the transformation occurs at about 0.5 GPa lower pressure relative to Mg_2SiO_4. We have carried out several in situ X-ray diffraction experiments on ringwoodite to Mg–perovskite + ferropericlase and backward transformations and found that post-spinel transformation boundary can be expressed as P (GPa) = − 0.0005 T (K) + 23.54 using the gold equation of state by Tsuchiya [T. Tsuchiya, First-principles prediction of the P–V–T equation of state of gold and the 660-km discontinuity in Earth's mantle, J. Geophys. Res. 108 (2003) doi: 10.1029/2003JB002446]. The interval for coexisting ringwoodite and Mg–perovskite was found to be 0.1–0.5 GPa. The discrepancy between our data and the depth of the seismic discontinuity (global average 654 km) is about 20 km at 1850 K. Based on the results of in situ measurements we confirmed that the difference in chemical composition between pyrolite and Mg_2SiO_4 cannot modify the Clapeyron slope of the post-spinel transformation. Using experimental data and assuming the average mantle temperature 1850 K at 660 km we can account for only a half of variations in the depth of the 660-km discontinuity in subduction zones and at hot spots. An additional explanation for the observed seismological variations at the 660-km discontinuity is required and may reflect influence of other minor components or volatiles.

Keywords: high pressure; phase transformation; mantle; ringwoodite; Mg–perovskite; 660-km discontinuity

1. Introduction

The 660-km seismic discontinuity is one of the most important phase boundaries in the Earth's interior. It divides upper and lower mantles and is usually attributed to the post-spinel transformation (hereafter

* Corresponding author. Tel.: +81 22 7956687; fax: +81 22 7956662.
E-mail address: klitasov@ganko.tohoku.ac.jp (K. Litasov).

0012-821X/$ - see front matter © 2005 Elsevier B.V. All rights reserved.
doi:10.1016/j.epsl.2005.08.001

PST), ringwoodite (or Mg_2SiO_4 spinel, hereafter Rw)=Mg–perovskite (Mpv)+ferropericlase (Fpc), in Mg_2SiO_4 or in a peridotite mantle composition. Many researchers have investigated the phase relations of PST in Mg_2SiO_4 [1–8] and peridotite systems [9–11] using both quench multianvil experiments and in situ X-ray diffraction using multianvil or diamond anvil techniques.

Ito and Takahashi [2] reported a detailed study of PST in the Mg_2SiO_4–Fe_2SiO_4 system by using a multianvil apparatus and concluded that for composition of Fo_{90}, the phase boundary is located at 22.9 GPa and 1850 K (an average mantle temperature at 660 km), which corresponds to 660 km depth and has a steep negative Clapeyron slope of −3.0 MPa/K. This boundary is widely cited for the interpretation of the observed 660-km discontinuity. However, at that time they were not able to determine the pressure values at high temperature precisely, since pressures were estimated by calibration against the press load.

Recent advances in synchrotron radiation have allowed us to determine the phase boundaries by in situ X-ray diffraction measurements. Irifune et al. [4] studied PST in the Mg_2SiO_4 system using in situ X-ray diffractometry and found essentially the same negative Clapeyron slope as observed in [2]. However, they located the phase boundary at about 2 GPa lower pressure, which was calibrated by the equation of state (EOS) of gold by Anderson et al. [12] (hereafter AA-89). Further, Chudinovskikh and Boehler [5] and Shim et al. [6] have also questioned their data by using measurements by a laser-heated diamond anvil cell (DAC) and showed that PST occurs at a pressure that is generally consistent with the depth of the 660-km discontinuity.

Since diamond anvil cell experiments could not provide precise data on pressure and Clapeyron slope of the phase transformation, Katsura et al. [7] and Fei et al. [8] re-examined the PST boundary in Mg_2SiO_4 using similar techniques to those used previously [4] but with more rigorous evaluation of kinetics of the transformation and pressure calibration scales. Katsura et al. [7] observed that the PST boundary is located at 22 GPa and 1850 K and has gentle negative Clapeyron slope of −0.4 MPa/K using the pressure calibration by AA-89, whereas Fei et al. [8] placed the PST boundary at 23 GPa and 1850 K with more pronounced negative Clapeyron slope of −1.3 MPa/K using EOS for MgO by Speziale et al. [13] (hereafter MS-01).

On the other hand, both the studies by Katsura et al. [7] and Fei et al. [8] created significant complexities to explain the topography of the 660-km seismic discontinuity in the subduction zones, where it may be depressed up to 45 km, and in the vicinity of hot spots/mantle plumes, where it can be elevated up to 20 km [e.g. [14–16]]. The seismological observations are consistent with data for the Clapeyron slope of PST calculated by Bina and Helffrich [17] (2.0 MPa/K) and experiments by Ito and Takahashi [2] (3.0 MPa/K). New data by Fei et al. [8] may account for only a half of the variations in a depth of the 660-km discontinuity of about +20 and −10 km. There are several possible explanations for this discrepancy: (1) problems with the experimental techniques, e.g. the pressure calibration, influence of pressure on electromotive forces (emf) of the thermocouple, and a systematic temperature gradient across the charge; (2) influence of other major and minor components, the difference in Mg/Si ratio between a peridotite mantle and Mg_2SiO_4, and variation in Mg number; and (3) shift of the phase boundary by adding volatiles.

Very recently, Nishiyama et al. [11] determined the PST boundary in primitive peridotite (pyrolite) composition and placed it at 22.0 GPa and 1873 K using MgO pressure scale by Matsui et al. [18] (which is generally consistent with MS-01). However, their measurements were made at constant temperature (1873 K), therefore they did not determine the Clapeyron slope of the transformation. In this study, we have investigated the phase relations in CaO–MgO–FeO–Al_2O_3–SiO_2 pyrolite obtained by in situ X-ray diffraction experiments at 20–25 GPa and temperature up to 2200 K. In addition, some quench experiments with long duration time were carried out for careful determination of the equilibrium phase compositions. With the help of these results we examine the influence of compositional changes on the PST boundary and its Clapeyron slope and discuss topography of the 660-km discontinuity.

2. Experimental

In situ X-ray diffraction experiments were conducted at the synchrotron radiation facility ‘SPring-

8' in Hyogo prefecture, Japan. We used a Kawai-type multianvil apparatus, 'SPEED-1500', installed at a bending magnet beam line BL04B1. Energy-dispersive X-ray diffractometry was conducted with a horizontal goniometer using white X-rays. Incident X-ray were collimated to form a thin beam of 0.05 mm in horizontal and 0.2 mm in the vertical dimensions by tungsten carbide slits and directed to the sample through pyrophyllite gaskets. A Ge solid-state detector was used and connected to 4096-channel analyzer, which was calibrated by using characteristic X-rays of Cu, Mo, Ag, Ta, Pt, Au, and Pb. Exposure times were 100 to 500 s. The diffraction angle (2θ) was ca. 5.5°. The diffraction angles were calibrated before compression for each run using d values of X-ray diffraction peaks and unit cell parameters of gold (a_0=4.0786 Å). The diffraction angles were determined with uncertainty of less than 0.0005°.

Starting material was prepared by a mixture of synthetic pyrolite glass and the gold with a 20:1 weight ratio. Five-component pyrolite glass was prepared by mixing the oxide and carbonate compounds and heating in an oven for 30 min at 1723 K under controlled oxygen fugacity to remove CO_2 and reduce Fe^{3+} to Fe^{2+}. The electron microprobe analyses and back-scattered electron images of the quenched glass indicate that it contains less than 20% by weight of forsterite crystals. The starting material is comparable with those used in previous studies of pyrolite compositions (Table A1, *see online version of this paper*).

The truncated edge length of the WC anvil was 2.0 mm. A cross-section of the sample assembly is shown in Fig. 1. The sample assembly was composed of a Co-doped MgO pressure medium, a cylindrical $LaCrO_3$ heater, molybdenum electrodes, and a graphite sample capsule isolated from the electrodes by MgO insulators. Temperature was monitored by a W3%Re–W25%Re thermocouple with a junction located at nearly the same position as where the X-rays pass through the sample. The temperature gradient in the sample capsule was inferred to be about ±50 °C [19]. The effect of pressure on the emf of thermocouple was ignored during the experiments.

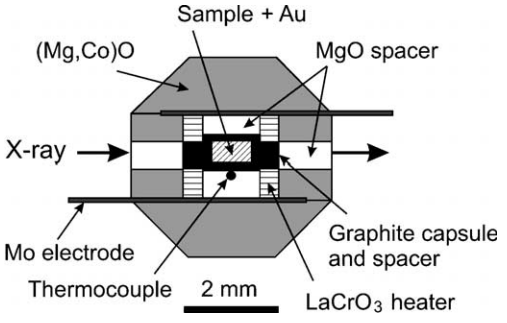

Fig. 1. The furnace assembly used for in situ X-ray diffraction experiments.

In the sample Per-4 we placed MgO+Au pressure marker (with a 10:1 weight ratio) between the thermocouple and sample and separated this pressure marker from the sample by a thin graphite disc. After compression we could measure X-ray diffraction patterns of sample+pressure marker.

For each experiment the cell assembly was first compressed to the desired press load at an ambient temperature and then heated gradually to the target temperature. This temperature was maintained before obtaining the clear Rw- or Mpv-bearing pattern. Thereafter, while continuously taking the diffraction patterns, temperature and the press load were increased and decreased, following complex P–T pass.

During the experiments the generated pressure at high temperature was calculated from the unit cell volume of gold using EOS by Tsuchiya [20] (hereafter AT-03). However, we placed pressures calculated using other EOS for Au and MgO to Table 1 and Fig. 2. Typically, five diffraction lines (111), (200), (220), (311), and (222) of Au or MgO were used to calculate pressure. Uncertainty of unit cell volume of Au or MgO determined by least squares method gives 0.1–0.2 GPa uncertainty in pressure. Pressure calibration is critical to assign the phase transition boundary and determine Clapeyron slope. However, there are huge uncertainties of pressure estimation caused by the differences of the equation of states of Au, Pt, MgO and other pressure markers at 20–25 GPa (e.g. [21]). The details of the pressure calibration using different EOS are discussed in Section 4.1.

Some additional quench experiments with the same sample configuration were carried out using a 3000-ton Kawai-type multianvil apparatus installed at Tohoku University. The pressure calibration was made using results of in situ experiments and is generally consistent with pressure versus load calibration using semiconductor to metal transitions at room temperature and PST in Mg_2SiO_4 [7,8] at high temperatures.

Table 1
Experimental conditions and results

Sample number	T (K)	V_{Au} (Å^3)	P [20] (GPa)	V_{MgO} (Å^3)	P [13] (GPa)	Reaction, run products
Sample Per-1						
Per-1-07	1273	63.29 (4)	21.1 (2)			RW
Per-1-11	1673	63.89 (1)	21.7 (1)			RW
Per-1-12	1773	64.06 (2)	21.8 (1)			RW
Per-1-13	1773	63.96 (3)	22.1 (1)			RW
Per-1-14	1773	63.79 (2)	22.7 (1)			RW+MPV
Per-1-17	1773	63.63 (1)	23.3 (1)			RW+MPV
Per-1-21	1773	63.55 (4)	23.6 (2)			RW→MPV
Per-1-24	1773	63.32 (1)	24.5 (1)			RW→MPV
Per-1-25	1573	63.16 (3)	23.8 (1)			RW→MPV
Per-1-30	1573	63.22 (2)	23.5 (1)			RW+MPV
Per-1-34	1573	63.39 (4)	22.9 (2)			RW+MPV
Per-1-35	1573	63.47 (3)	22.6 (1)			RW
Per-1-37	1573	63.52 (2)	22.4 (1)			RW
Per-1-38	1673	63.58 (2)	22.8 (1)			RW+MPV
Per-1-39	1688	63.79 (2)	22.2 (1)			RW
Per-1-45	1873	64.19 (2)	21.2 (1)			RW
Per-1-50	2073	64.55 (2)	22.3 (1)			RW
Per-1-51	2173	64.71 (3)	22.5 (1)			Wd (RW)→MPV
Sample Per-2						
Per-2-06	1273	63.41 (2)	22.1 (1)			RW
Per-2-08	1673	63.94 (2)	21.5 (1)			RW
Per-2-13	1973	64.40 (1)	22.1 (1)			RW
Per-2-14	1973	64.29 (2)	22.5 (1)			RW
Per-2-15	1953	64.15 (4)	22.8 (2)			RW+MPV
Per-2-18	1933	63.99 (5)	23.3 (2)			RW+MPV
Per-2-25	1973	63.98 (4)	23.6 (2)			RW→MPV
Per-2-26	1973	63.86 (3)	24.0 (1)			RW→MPV
Per-2-29	1973	63.45 (6)	25.5 (2)			MPV
Sample Per-3[a]						
Per-3-06	1273	63.49 (3)	20.3 (1)		20.7	RW
Per-3-08	1573	64.00 (2)	20.6 (1)		21.0	RW
Per-3-15	1573	63.43 (1)	22.7 (1)		23.1	RW
Per-3-16	1623	63.51 (1)	22.8 (1)		23.2	RW+MPV
Per-3-18	1623	63.42 (1)	23.1 (1)		23.5	RW+MPV
Per-3-20	1673	63.40 (2)	23.4 (1)		23.8	RW+MPV
Per-3-22	1673	63.28 (4)	24.0 (2)		24.4	RW→MPV
Sample Per-4						
Per-4-12	1273	62.84 (1)	22.9 (1)	68.27 (5)	23.6 (2)	MPV
Per-4-14	1473	63.14 (2)	23.2 (1)	68.58 (6)	23.9 (3)	MPV
Per-4-19	1673	63.29 (2)	23.9 (1)	68.85 (4)	24.3 (2)	MPV
Per-4-23	1873	63.63 (1)	24.2 (1)	69.27 (3)	24.2 (1)	MPV
Per-4-30	1873	63.87 (2)	23.3 (1)	69.44 (5)	23.7 (2)	MPV
Per-4-31	1873	63.94 (1)	23.0 (1)	69.51 (5)	23.5 (2)	MPV
Per-4-32	1873	63.96 (1)	23.0 (1)	69.53 (8)	23.4 (3)	MPV
Per-4-33	1873	63.97 (1)	22.9 (1)	69.66 (5)	23.0 (2)	MPV
Per-4-34	1873	64.04 (2)	22.7 (1)	69.74 (8)	22.8 (3)	RW
Per-4-35	1873	64.15 (1)	22.3 (1)	69.89 (4)	22.3 (1)	RW
Per-4-36	1873	64.21 (2)	22.1 (1)	70.10 (5)	21.7 (2)	RW

Table 1 (*continued*)

Sample number	T (K)	V_{Au} (Å^3)	P [20] (GPa)	V_{MgO} (Å^3)	P [13] (GPa)	Reaction, run products
Quench experiments						
K-247	2173		22.6			Wd, Gt, Cpv, Fpc
K-251	1873		23.3			Rw, Gt, Mpv, Cpv, Fpc
K-243a	1873		25.4			Mpv, Cpv, Fpc, Gt

RW, ringwoodite-bearing assembly (ringwoodite+garnet+Ca–perovskite); MPV, Mg–perovskite-bearing assembly (Mg–perovskite+ferropericlase+Ca–perovskite+garnet). Wd, wadsleyite; Gt, garnet; Cpv, Ca–perovskite; and Fpc, ferropericlase.
Run duration for quench experiments K-247, K-251, and K-243a are 3, 12 and 12 h, respectively.
[a] MgO pressures for Per-3 are calculated from values by Au EOS using data from [11,21] and our unpublished data.

Recovered samples were polished and examined by an electron microprobe (JEOL Superprobe JXA-8800) at Tohoku University. An acceleration voltage of 15 kV and 10 nA specimen current was used for the analyses.

3. Results

We have performed four successful X-ray diffraction experiments at pressures between 20 and 26 GPa and temperatures up to 2200 K (Table 1 and Fig. 2). Irifune et al. [4] and Katsura et al. [7] noted difficulty in initiating the dissociation of Rw to Mpv+periclase because Rw formed at high P–T conditions is very inert. Katsura et al. [7] used inverse run procedure and observed the phase transformation from Mpv- to Rw-bearing assemblage during isothermal decompression. In the present work we used isothermal compression of Rw-bearing assemblage in three runs and found that nucleation of Mpv occurred consistently in all runs in the temperature range of 1573–1973 K. This might be connected with existence of untransformed glass in Rw-bearing assemblage, which could enhance nucleation of Mpv or differences in kinetics due to the multi-component system assembly and the existence of other phases (garnet and Ca–perovskite). In one run (Per-4) we used inverse transformation from Mpv- to Rw-bearing assemblage and found reliable consistency with other runs (Fig. 2).

Tables A2 and A3 (*see online version of this paper*) summarize d values, relative intensities, indices of diffraction lines, and unit cell parameters of the phases at ambient conditions and after the experiment. Most diffraction lines can be indexed based on Mpv, Ca–perovskite, Fpc, Rw, garnet, and gold pressure marker. One unidentified peak was observed in several patterns at 1.940 Å.

In run Per-1, presence of Rw, majorite garnet and Ca–perovskite was confirmed at 22.1 GPa and 1773 K (Figs. 2 and 3). With increasing the pressure load we observed appearance of Mpv and Fpc at 22.7 GPa and 1773 K. Following further increase of pressure we observed growth of Mpv and Fpc peaks and diminishing of Rw peaks in X-ray diffraction patterns. However, between 22.7 GPa and about 23.3 GPa after re-equilibration no reaction proceeds further during at least 30 min at fixed conditions. This may indicate the coexistence field of Rw and Mpv+Fpc. At pressures above 23.3 GPa, fast transformation from Rw- to Mpv-bearing assemblage was occurred. We

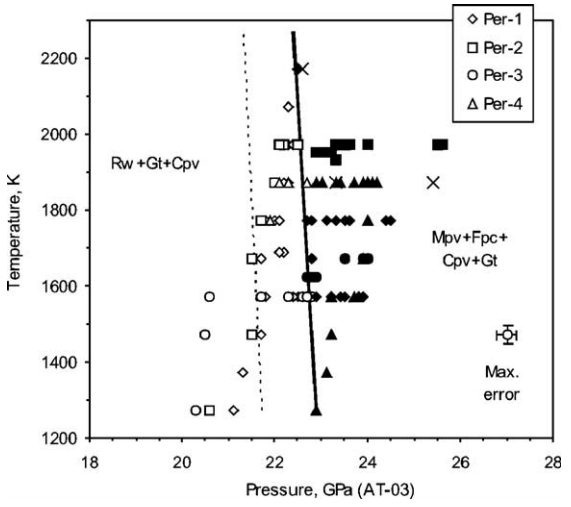

Fig. 2. Post-spinel transformation boundary in anhydrous pyrolite determined by in situ X-ray diffraction experiments using pressures calculated by AT-03. *Open symbols*, Rw, *filled symbols*, Mpv+Fpc., and *X*, quench experiments. *Solid lines*, appearance of Mpv.

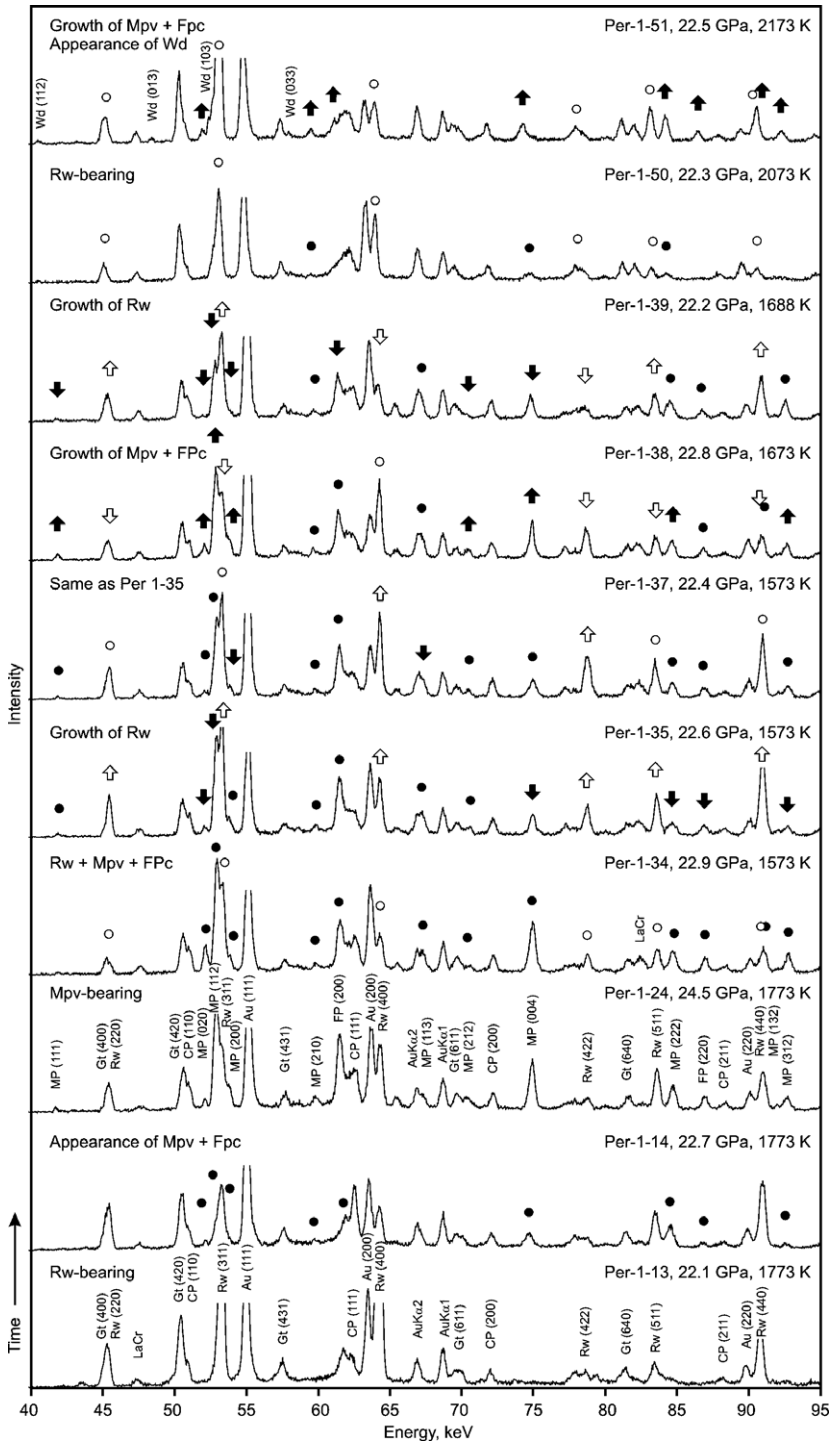

Fig. 3. Representative X-ray diffraction patterns of the sample Per-1 at the indicated *P–T* conditions using AT-03. Peak identifications are Rw, ringwoodite; MP, Mg–perovskite; FP, ferropericlase; CP, Ca–perovskite; Gt, garnet; Au, gold; and LaCr, $LaCrO_3$. *Open arrows and circles*, ringwoodite; *filled arrows and circles*, Mg–perovskite and ferropericlase.

collected a Mpv+Fpc-bearing pattern with minor Rw peaks at 24.5 GPa and 1773 K (Figs. 2 and 3). We then decreased the temperature to 1573 K and decreased pressure to obtain the Rw-bearing pattern again. We observed fast growth of Rw at 22.6 GPa and 1573 K. Mpv and Fpc almost disappeared when temperature was increased from 1573 to 2073 K. However at 22.5 GPa and 2173 K Mpv peaks grew rapidly and few wadsleyite peaks appeared (Fig. 3). This observation could be important to position the triple point for coexisting Rw+wadsleyite+(Mpv+Fpc). However, unfortunately we have insufficient experimental data points to determine the slope and pressure of wadsleyite to Mpv+Fpc transformation precisely.

In run Per-4, we observed transformation from Mpv to Rw between 22.9 and 22.7 GPa at 1873 K. The transformation was started at little higher pressure than that from Rw to Mpv. This also confirms a coexistence field of Rw+Mpv+Fpc, however the pressure interval of coexistence is narrower (0.1–0.2 GPa) than estimated from the other runs (about 0.5 GPa).

The results of other experiments are consistent with those of Per-1 and Per-4 and indicate very gentle negative Clapeyron slope of the PST boundary. Fig. 2 summarizes the results of phase relations in pyrolite as a function of pressure. The phase boundary for appearance of Mpv can be expressed as P (GPa) = − 0.0005 T (K) + 23.54 using pressures calculated by AT-03. The

Table 2
Representative compositions (wt.%) of minerals in the recovered samples

	Per-2					Per-3				
	Mpv	Cpv	Fpc	Gt	Rw	Mpv	Cpv	Fpc	Gt	Rw
SiO_2	57.17	50.86	0.72	48.40	41.06	58.86	51.43	1.08	47.62	40.87
Al_2O_3	2.05	1.63	1.34	14.05	0.52	0.74	1.12	0.42	13.18	0.03
FeO	5.62	1.03	23.81	6.60	9.88	3.03	0.89	25.76	8.52	10.02
MgO	35.67	2.24	73.16	25.08	47.40	37.53	1.96	72.24	19.35	49.03
CaO	0.34	44.49	0.08	5.40	0.39	0.32	45.19	0.11	10.78	0.31
Total	100.85	100.25	99.11	99.53	99.25	100.48	100.59	99.61	99.45	100.26
Mg#	91.9	79.5	84.6	87.1	89.5	95.7	79.7	83.3	80.2	89.7
Si	0.973	0.975	0.005	0.852	1.012	0.993	0.983	0.008	0.860	0.999
Al	0.041	0.037	0.012	0.292	0.015	0.015	0.025	0.004	0.281	0.001
Fe	0.080	0.017	0.150	0.097	0.204	0.043	0.014	0.163	0.129	0.205
Mg	0.905	0.064	0.821	0.658	1.740	0.944	0.056	0.814	0.521	1.787
Ca	0.006	0.914	0.001	0.102	0.010	0.006	0.926	0.001	0.209	0.008
Total	2.006	2.006	0.989	2.002	2.981	2.000	2.004	0.990	1.999	3.000
Density, g/cm^3	4.18	4.21	3.94	3.64	3.61	4.13	4.21	3.97	3.72	3.63

	K-247				K-251				K-243		
	Mpv	Fpc	Gt	Wd	Mpv	Fpc	Gt	Rw	Mpv	Fpc	Gt
SiO_2	55.91	0.51	49.78	40.61	57.25	1.12	47.81	40.47	54.25	1.04	46.92
Al_2O_3	3.44	1.66	12.32	0.00	1.61	0.92	13.55	0.09	4.93	1.13	16.03
FeO	5.92	22.59	5.10	9.43	4.84	24.10	6.26	10.75	7.01	19.67	6.56
MgO	34.80	74.57	26.24	49.22	36.43	74.09	23.47	48.33	33.47	77.44	24.54
CaO	0.34	0.05	6.96	0.06	0.26	0.03	8.45	0.17	0.30	0.08	5.21
Total	100.41	99.38	100.40	99.32	100.39	100.26	99.54	99.81	99.96	99.36	99.26
Mg#	91.3	85.5	90.2	90.3	93.1	84.6	87.0	88.9	89.5	87.5	87.0
Si	0.958	0.004	0.867	0.999	0.976	0.008	0.849	0.997	0.939	0.008	0.828
Al	0.070	0.015	0.254	0.000	0.032	0.008	0.284	0.003	0.101	0.010	0.335
Fe	0.085	0.141	0.074	0.194	0.069	0.150	0.093	0.222	0.101	0.121	0.097
Mg	0.889	0.829	0.681	1.805	0.926	0.821	0.621	1.775	0.863	0.848	0.646
Ca	0.006	0.000	0.130	0.002	0.005	0.000	0.161	0.004	0.006	0.001	0.099
Total	2.007	0.989	2.006	3.001	2.008	0.988	2.009	3.001	2.010	0.987	2.004
Density, g/cm^3	4.19	3.91	3.63	3.61	4.16	3.93	3.66	3.64	4.21	3.85	3.63

See Table 1 for abbreviations.

transitional interval for coexistence of Rw and Mpv was found to be narrow (0.1–0.5 GPa).

Hirose [10] reported existence of akimotoite (ilmenite-structured $MgSiO_3$ phase) in pyrolite at 1873 K and 20–21 GPa. We did not observe akimotoite in our experiments and our results are broadly consistent with phase changes observed in pyrolite by Wood [22], Nishiyama and Yagi [23] and Nishiyama et al. [11].

In order to obtain equilibrium phase compositions, additional quench experiments were carried out at pressures of 22.5–25.5 GPa and temperatures of 1873–2173 K. The composition of the phases after in situ and quench experiments are summarized in Table 2 and are consistent with those previously reported for observed minerals [10,11,22,23]. Rw has Mg#=89–90. Garnet contains 12–16 wt.% Al_2O_3 and 5–6 wt.% CaO. Garnet in the sample Per-3 contains 10.8 wt.% CaO and the modal amount of Ca–perovskite is very low in this sample (0.5 wt.%). This might be caused by a low initial pressure after compression (20.6 GPa at 1573 K) when the primary sample assembly was crystallized outside the Ca-perovskite stability field. Then, with increasing pressure partial transformation of garnet to Ca-perovskite-bearing assembly occurred slowly. However, this modal variation had minor effect on the pressure of Mpv appearance since the results of Per-3 are consistent with the other runs.

Mpv near the transition boundary has a low Al_2O_3 content (0.7–1.6 wt.%) and has high Mg#=93–96. Fpc has Mg#=83–86 and contains 0.4–1.7 wt.% Al_2O_3. Fig. 4 shows the relation between Al content in Mpv and K^{app} ($=X_{Fe}^{Mpv}X_{Mg}^{Fpc}/X_{Mg}^{Mpv}X_{Fe}^{Fpc}$, where $X_{Fe}^{Mpv}=(Fe^{2+}+Fe^{3+})/(Fe^{2+}+Fe^{3+}+Mg)$), which was defined in [22,23]. We can see a trend of increasing K^{app} with increasing the Al content of Mpv. It was shown that small amount of Al_2O_3 (<2.5 wt.%) in Mpv has only a small effect on K^{app}, whereas the presence of a larger amount of Al_2O_3 in Mpv affects it considerably [11], i.e. the relation between the Al content in Mpv and K^{app} is non-linear. However, our samples, together with some data from other studies [e.g. [10,22]] show that this relation tends to be linear up to the pressures of complete garnet dissociation, when Mpv contains about 5 wt.% Al_2O_3 (Fig. 4).

Nishiyama et al. [11] noted also that the Al content of Mpv increases with increasing pressure. We can emphasize that Al_2O_3 content of Mpv close to the PST pressure increases with increasing temperature (1.6 wt.% Al_2O_3 at 1873 K and 3.4 wt.% Al_2O_3 at 2173 K).

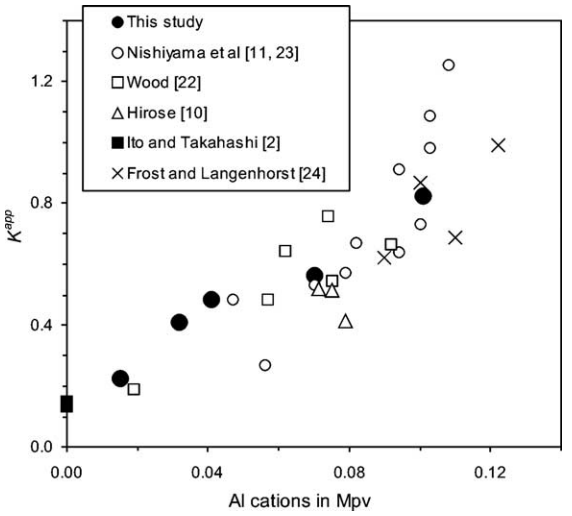

Fig. 4. Al content in Mg–perovskite versus apparent partition coefficient between Mg–perovskite and ferropericlase determined in this work and previous studies. Data from [2,10,11,22–24] and this study.

4. Discussion

4.1. Pressure calibration in multianvil in situ studies

In order to constrain the phase boundaries at high pressures we must establish a pressure marker with a reliable EOS. Au, Pt, and MgO are typically used for in situ high-pressure observation by multianvil apparatus [e.g. [21]]. Unfortunately there is no consistency between different pressure scales. For instance, the calculated pressure differences between different EOS of Au [12,20,25,26] may be as large as 2.5 GPa at 25 GPa and 2000 K. It was shown that the AA-89 underestimates pressure at least by about 1.5 GPa at 20 GPa and high temperatures [27]. Calibration of the pressure effect on the anharmonicity of gold indicates that AA-89 may underestimate the pressure by about 1 GPa at 1000 K and 2–3 GPa at 2000 K at 20 GPa [28]. Jamieson's Au pressure scale [25] is consistent with location of the PST boundary at 660 km along an average mantle geotherm proposed

by Akaogi et al. [29]. However, this EOS for Au is thought to overestimate pressure [27] due to (a) stiffer compression curve obtained from Hugoniot data relative to new quasihydrostatic compression data and (b) too high value of the assumed Grüneisen constant.

Recently Fei et al. [21] made comprehensive review of different pressure scales and calibrate Au and Pt scales based on MgO standard using MS-01. They reported that pressures calculated from the MS-01 are about 1.5 GPa higher than those from AA-89. We found that, the pressures calculated by MS-01 are generally consistent with those by AT-03. By using the data of Fei et al. [21], Nishiyama et al. [11] and our unpublished results we estimated that P (MS-01) − P (AT-03) = 0.08 ± 0.36 GPa in the pressure range 20–25 GPa and temperatures between 1500 and 2200 K. However, at lower temperatures of 1200–1500 K the difference P (MS-01) − P (AT-03) may exceed 0.4 GPa (Table 1).

The pressures calculated using AT-03 and by recalculation to MS-01 (since we performed direct measurements of MgO pressure marker only in one run) may be the most reliable for present experiments (Table 1) as they give highest pressures for PST, which is more consistent with 660-km discontinuity. Additionally, we placed unit cell volumes of Au and MgO at high-PT conditions in Table 1 for possible pressure re-estimation if newly corrected pressure scales become available.

4.2. Influence of pressure on emf of thermocouple and temperature uncertainty

There is little systematic information about influence of pressure on electromotive force or voltage of W/Re thermocouples. Li et al. [30] showed that the difference between Pt–Rh (type S) and W–Re (type C) thermocouples at 15 GPa is about −15 K at 1273 K and +40 K at 2173 K. Extrapolation of this data to 20 GPa indicates that we can expect deviation of the PST boundary to lower pressure at highest temperatures (Fig. 5) and pressure effect on thermocouple may increase Clapeyron slope to 0.10 MPa/K. Moreover, PST line may deviate from the linear trend by assumed corrections, which is consistent with calculations by Bina and Helffrich [17]. It should be noted that data by Li et al. [30] is relative and depends on temperature variations in type S thermocouple. Therefore, application of these data for the present experiments is not unequivocal and we have emphasized just a possibility that the pressure effect on thermocouple may have evident influence on the Clapeyron slope of transformation.

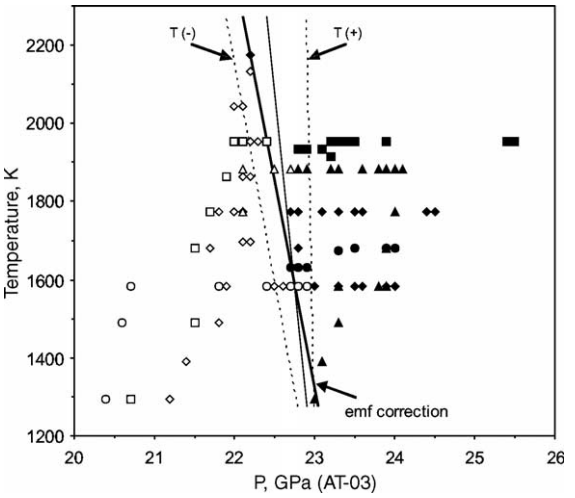

Fig. 5. Possible corrections of PT-conditions calculated using AT-03 by influence of pressure on emf of the thermocouple (*bold line*) estimated using data by Li et al. [30] and due to temperature uncertainties (*dashed lines*). Thin line is PST without corrections. See Fig. 2 for other symbols.

In Fig. 5 we showed also pressure variations due to temperature uncertainty of ± 100 K at 2173 K and ± 10 K at 1273 K, which may be caused by temperature gradient across the charge [19]. The influence of temperature uncertainty should be insignificant because position of X-ray pass and junction of thermocouple located at the distance of about 0.2 mm, i.e. temperature difference may not exceed 50 K.

4.3. Comparison with previous data

We have compared present data with recent studies of PST in Mg_2SiO_4 and pyrolite using both multianvil and diamond anvil cell experiments in Table 3 and Fig. 6. Two parameters should be representative for this comparison, which are as follows: (a) pressure of PST, which can be estimated via relation to 660 km at 1850 K (temperature proposed for average mantle by Akaogi et al. [29]) and (b) Clapeyron slope of the transformation boundary.

Most studies by in situ multianvil technique yield PST pressures that are significantly lower than that at 660 km (Fig. 6). First in situ data [4] for PST in

Table 3
Parameters for the post-spinel transformation boundary determined by different authors

Sample	Refs.	EOS	*a*	*b*	*P* (GPa)[a]	*D* (km)
Pyrolite	This work	AA-89 [12]	0.04	22.259	21.5	6
		AT-03 [20]	0.05	23.537	22.6	8
		Au [25]	0.03	23.918	23.4	5
		Au [26]	0.02	22.755	22.4	3
		MS-01 [13]	0.08	24.418	22.9	12
		Emf correction[b]	0.10	24.259	22.4	13
Mg_2SiO_4	[4]	AA-89 [12]	0.25	25.933	21.3	37
Mg_2SiO_4	[7]	AA-89 [12]	0.07	23.315	22.0	11
Mg_2SiO_4	[8]	AA-89 [12]	0.08	23.247	21.8	12
		MS-01 [13]	0.13	25.441	23.0	17
Pyrolite	[11]	AA-89 [12]			20.8	
		MgO [18][c]			22.0	
$(Mg, Fe)_2SiO_4$	[2]	Au [25][d]	0.30	28.619	22.9	45
Mg_2SiO_4	[5][e]	Ruby [31], SrB_4O_7[f]			23.0	
Mg_2SiO_4	[6][e]	Ruby [31], Pt[f]			23.6	
Mg_2SiO_4	[17]	Calculated[g]	0.20	27.300	23.6	30

P (GPa)$=-aT$ (K)$/100+b$.
D, calculated depression of the 660-km discontinuity at the temperature of the model cold slab. The values of elevations of 660-km discontinuity in hot mantle plumes are about $D/2$ (see Fig. 6).
[a] At 1850 K.
[b] Assumed pressure corrections for emf of thermocouple based on AT-03 (see Fig. 5).
[c] This pressure scale is consistent with MS-01 within 0.2 GPa uncertainty.
[d] Quenching experiments using a multianvil apparatus.
[e] DAC experiments.
[f] To account thermal pressure.
[g] By optimization using calorimetric measurements of Akaogi et al. [3,29].

Mg_2SiO_4 using AA-89 lead to confusion because the PST was located 2 GPa lower than the pressure at 660 km. It therefore did not explain the 660-km seismic discontinuity. Following studies by DAC [5,6] and multianvil with an improved technique [7] shifted this boundary to the higher pressures.

PST obtained through in situ measurements by Fei et al. [8] is similar to that by Katsura et al. [7] using Au EOS (Fig. 6). The PST boundary for Mg_2SiO_4 reported by Fei et al. [8] using MS-01 is closest to 660 km: $\Delta P_{660}=(P_{660\ \mathrm{km}}-P_{\mathrm{measured}}$ at 1850 K$)=0.6$ GPa. In this study we obtained $\Delta P_{660}=1.0$ GPa using AT-03, whereas $\Delta P_{660}=0.8$ GPa if we recalculate our data to MS-01. Fei et al. [8,33] noted also that the transition pressure in KLB-1 peridotite is about 0.8 GPa lower than that in Mg_2SiO_4, however they did not mention the pressure calibration methods and temperatures. Consequently, their pressure for PST may be 0.3–0.5 GPa lower than that in our study at temperature 1850 K (Fig. 6). Nishiyama et al. [11] placed phase boundary at 20.8 GPa using AA-89, which is 0.7 GPa lower than our results. Comparison of our data with those in [11] using the MgO pressure scale by Matsui et al. [18] or MS-01 gives 0.9 GPa difference. This discrepancy cannot be fully understood at present because Nishiyama et al. [11] made experiments only at 1873 K and results by Fei et al. [33] have been published only in the form of abstract. We should note that Nishiyama et al. [11] used a WC+diamond sheet heater. Although they placed Mo discs to distribute temperature evenly, use of the sheet heater may cause systematic difference in the temperature between the thermocouple and the sample. The run duration may not have an influence, since run duration of the experiments by Nishiyama et al. [11] was similar to our experiments. However, consistency among our runs and absence of Mpv at high temperatures (1900–2100K) and 22.2 GPa (AT-03, Fig. 2), where we do not expect problems on kinetics of transformation, allow us to suggest that our results are more reliable than those in [11]. There is also a possibility of influence of minor components like Cr_2O_3 or Na_2O on the phase boundary and discrepancy between our data

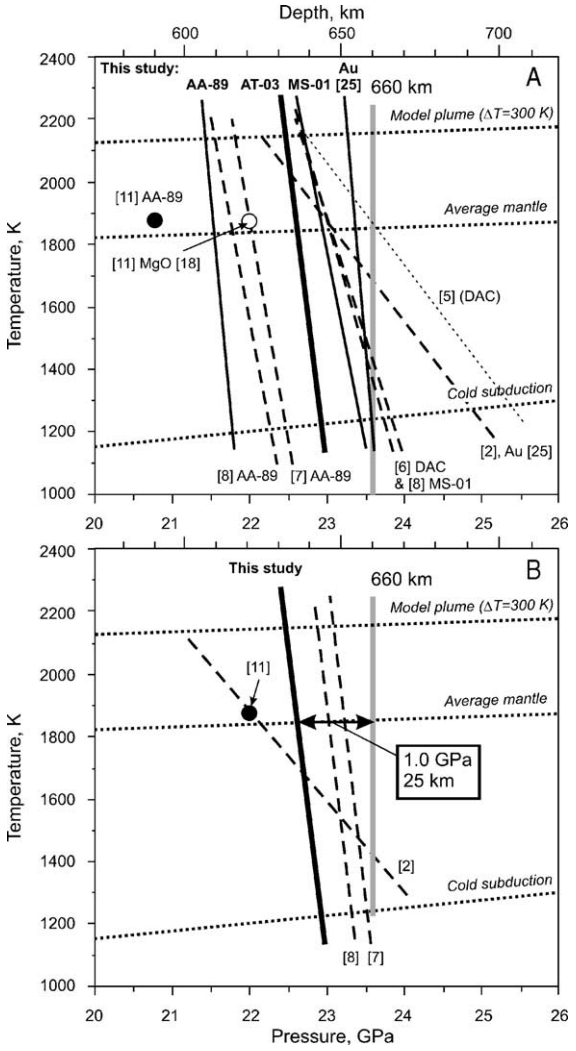

Fig. 6. Comparison of PST boundary obtained with present study with previous data obtained using different Au and MgO pressure scales (A) and those normalized to Au pressure scale by Tsuchiya [20] (B). Average mantle geotherm is after Akaogi et al. [29]. Cold subduction geotherm is after Kirby et al. [32]. DAC, diamond anvil cell experiments. Circles and bold lines, data for pyrolite. Dashed lines, data for Mg_2SiO_4 and $(Mg_{0.9}Fe_{0.1})_2SiO_4$ [2]. The discrepancy between experimental data and observed depth of seismic discontinuity is shown.

and those by Nishiyama et al. [11] may be caused by differences in starting composition (Table A1, see online version of this paper). Currently our results for PST in pyrolite show closest consistency with 660-km discontinuity measured by in situ X-ray diffraction in multianvil experiments. It may be located between 22.6 and 22.9 GPa at 1850 K (Table 3).

The results obtained by Shim et al. [6] for Mg_2SiO_4 using DAC are very consistent with the data by Fei et al. [8] and indicate general agreement between multianvil and diamond anvil cell pressure calibrations. Data obtained by Chudinovskikh and Boehler [5] using DAC show a higher pressure of PST (Fig. 6), perfectly consistent with the 660-km seismic discontinuity and exceeding the pressure values by Fei et al. [8] and Shim et al. [6]. The results obtained by DAC however, have large temperature (100–200 K) and therefore pressure uncertainties and estimate the PST boundary roughly. DAC results are also very scattered to estimate the Clapeyron slope of PST.

Our experimental results suggest a very gentle negative Clapeyron slope of PST (from −0.8 to −0.2 MPa/K), which is consistent with data obtained in [7,8] for Mg_2SiO_4 using AA-89 (Table 3). However, data by Fei et al. [8] show steeper Clapeyron slope of PST (−1.3 MPa/K) if MS-01 is used for the pressure calibration. The results obtained by Ito and Takahashi [2] using quench experimental technique result in negative Clapeyron slope for PST (−3.0 MPa/K) that is too steep. Bina and Helffrich [17] estimated Clapeyron slope of PST to be −2.0 MPa/K performing optimization analyses using calorimetric data from [3,29]. They also noted that PST can deviate from linear trend and Clapeyron slope can be steeper at high temperature (−2.7 MPa/K at about 1900 K) than at lower temperature (−1.9 MPa/K at about 1400 K). Consistently, our data also permit slight deviation of the PST boundary from linear trend (see Figs. 2 and 5).

Based on the results of in situ measurements we conclude that the difference in chemical composition between pyrolite and Mg_2SiO_4 do not increase the negative Clapeyron slope of PST significantly and it may vary between −0.4 and −0.8 MPa/K using both the Au and MgO equations of state.

4.4. PST in pyrolite and the 660-km seismic discontinuity

The seismic discontinuity at the global average depth of 660 km has been attributed to PST [e.g. [2,14]]. For comparison between the experimental PST boundary and seismic observations we consider the following three major points: (1) the pressure/

depth of 660-km discontinuity; (2) application of the experimental Clapeyron slope for elevations and depressions of the 660-km discontinuity; and (3) sharpness of the discontinuity.

The average depth estimation for the 660-km discontinuity varies in the range of 650–670 km. Flanagan and Shearer [14] reported the average depth of 647 km by using SS travel times, however, after making corrections to topography, crustal structure, lateral S velocity variations, and some other factors they obtained 660 km global average. Recent observations by Gu et al. [34] indicate that the global average for the 660-km discontinuity is 654 km and this value is similar to that proposed earlier (e.g. [35]). If we accept 654 km as a global average, then the pressure discrepancy between PST observed in the experiments and that in seismic studies decreases by 0.2–0.3 GPa. Thus, discrepancy between our data (22.6–22.9 GPa at 1850 K) and the pressure of seismic discontinuity is about 1 GPa (20–25 km).

Mapping of the global topography on the transition zone velocity discontinuities shows variations in the depth of 660 km from about +20 km, for example, in the northern Pacific and Atlantic Ocean and South Africa to −20 km in the western Pacific and South America [14,16,34]. Lebedev et al. [36] proposed smaller variations in the range of ± 15 km. Regional studies of seismic discontinuities near subduction zones show slab-induced depression of 20–30 km on the 660-km discontinuity beneath Tonga [37] and up to a 50-km depression beneath Izu-Bonin [15,38,39]. Vidale and Benz [40] obtained depth perturbations of up to 30 km beneath the Tonga, Izu-Bonin, Marianas, and South American subduction zones. Several regional studies showed that the 660-km discontinuity elevates by 10–20 km in the areas related to Iceland [41], Hawaii [42], and South Pacific [43] due to the impact of plume-related upwelling.

Application of the Clapeyron slope obtained by experiments to the seismic observations may provide constraint for the average mantle geotherm. Previously, major arguments for the upper mantle geotherm were the relation between seismic discontinuities at the 410 and 660 km depths and the experimental phase transitions from olivine to wadsleyite (β-Mg_2SiO_4) and PST (e.g. [17,29]). Calculations of the density and seismic velocity profiles of a model pyrolite composition along this geotherm using available thermoelastic parameters of minerals [e.g. 9,44–46] suggest the consistency with seismological models, such as PREM [47] or Ak135 [48] (Fig. 7). However, it may not be possible to resolve a 100–200 K difference in the mantle geotherm comparing the calculated density, velocity profiles and seismological models because of the uncertainties in the modal proportions and thermoelastic parameters of constituent minerals. For instance, the value of density and velocity jump at 660 km varies from 3.5% [44] to 6–7% [[45], this work].

Majority of mantle geotherms calculated using thermoelastic parameters of minerals in the upper and lower mantle provide results (e.g. [49,50]) that are consistent with the geotherm by Akaogi et al. [29]. This geotherm is also consistent with observed heat flow and plate velocities at shallow levels of the mantle [51]. However, if we assume existence of water in the transition zone (e.g. [52]) and low-velocity zone of the upper mantle, the resulting geotherm could be lower [53].

Global tomography studies may indicate that the temperature difference between the hot mantle plumes and an average mantle is almost similar to the difference between the subduction zones and an average mantle. Assuming a maximum plume temperature below the solidus of dry pyrolite [54] an average mantle temperature at 660 km should be 1650–1750 K, which is 100–200 K lower than generally accepted geotherm (Fig. 6). Moreover, placing the mantle geotherm 100–200 K lower we have more consistency with our results for PST (22.8–23.1 GPa at 1650 K). However, regional seismological studies show that depressions of 660 km in the subduction zones are about two times larger than elevations in the hot regions. This is consistent with the widely accepted temperature model [29] for the upper mantle (Fig. 6).

If we assume an average mantle temperature 1850 K at 660 km we may explain only minor variations in the depth of 660 km using the experimental data (about +10 for hot and −20 km for cold regions of the mantle). Therefore, an additional explanation for larger variations is needed. This may include a delay of the phase transformation due to kinetics, or the influence of minor components, or volatiles. Study of kinetics of PST in Mg_2SiO_4 indicates that with 1 GPa overpressure the reaction Rw = Mpv + Fpc proceeds rapidly (completed during 10^4 years) at temperatures above 1000 K. Only for very cold slabs, with temperatures below

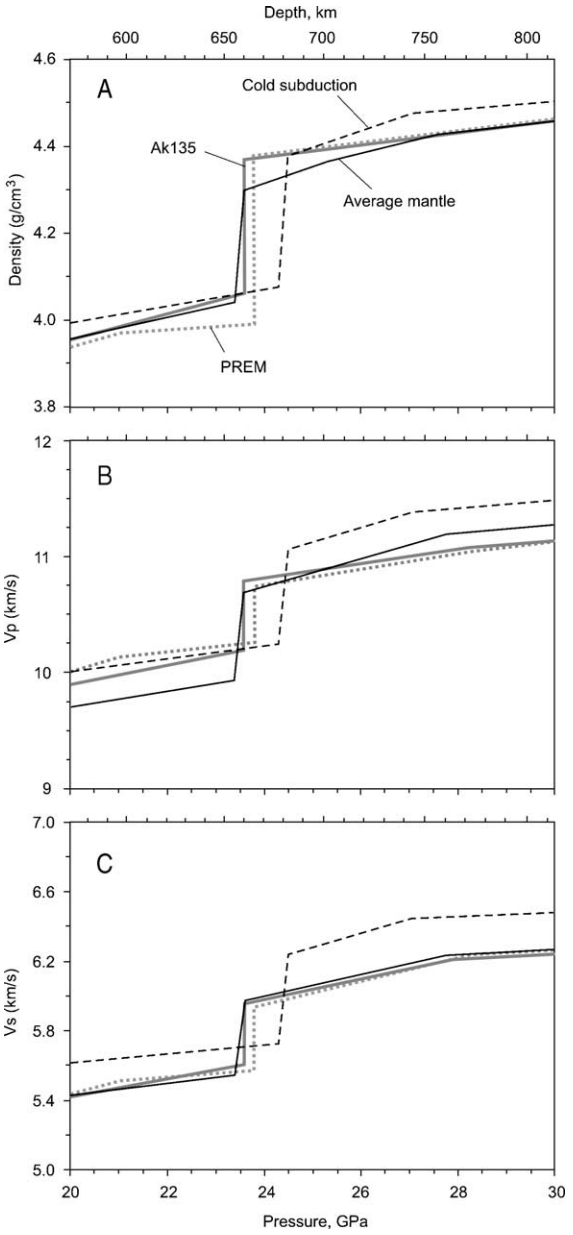

Fig. 7. Comparison of the simplified (no ilmenite) density (a) and seismic velocity (b and c) profiles of anhydrous pyrolite along the different geotherms corresponding to normal mantle and cold subduction slab (see Fig. 6). Density calculations were carried out along the geotherms using a third-order Birch–Murnaghan equation of state and the set of thermoelastic parameters after [45–56]. Mineral proportions in pyrolite were taken from [46]. PREM and Ak135 are the average mantle parameters of the seismic models after [47] and [48], respectively.

1000 K at the PST pressure, the reaction cannot be completed for 10^6–10^8 years [19]. Thus, we can expect a delay of transformation and shift of PST due to kinetics by about 1 GPa (corresponding to 20–25 km) only in hypothetically very cold slabs.

A more attractive hypothesis might be the presence of water. Since Rw contains up to 3 wt.% H_2O and Mpv and Fpc only 0–0.02 wt.% H_2O (e.g. [55–57]), we can expect a shift of the PST boundary to higher pressures if the subducting slabs contain considerable amount of water. Although quench experiments in Mg_2SiO_4+ H_2O indicate insignificant shift of PST to the higher pressures for 0.2 GPa [58], our newest data for pyrolite suggest possible shift of PST by water of at least 0.6 GPa at temperature of the hot subducting slabs [59].

Seismological data show that the 660-km discontinuity is sharp in most cases and does not exceed 5 km (0.2 GPa) (e.g. [60,61]. The pressure interval of coexisting Rw and Mpv+Fpc has been shown to vary in different experimental studies. Ito and Takahashi [2] reported it to be less than 0.1 GPa for $(Mg_{0.9}Fe_{0.1})_2SiO_4$. Wood [22] noted that chemographic relations of the coexisting phases near 22–23 GPa also suggest that PST takes place over a very narrow pressure interval. Whilst, Hirose [10] and Nishiyama et al. [11] determined relatively wide pressure range (0.5–0.7 GPa) for PST in pyrolite, our results for Rw to Mpv+Fpc transformation also suggest a field of coexistence of at least 0.5 GPa. However, reverse experiments showed narrow field of 0.1–0.2 GPa and very fast transformation from Mpv to Rw occurred even under minor overpressure. Although nucleation of Rw in reverse reaction may be controlled by the kinetics of transformation, this has not yet been investigated and we tentatively conclude that the pressure interval of coexisting Rw and Mpv+Fpc should be narrow and not exceed 0.5 GPa.

5. Conclusions

The 660-km seismic discontinuity in the Earth's mantle has been identified with the transformation of Rw to Mpv and Fpc. It has been pointed out that the transformation boundary has a significant negative Clapeyron slope (−3.0 MPa/K, [2]), which is responsible for depth variations of the 660-km discontinuity in subduction zones and hot mantle plumes. Recent

in situ X-ray diffraction studies in the Mg_2SiO_4 indicate that the negative slope of the boundary is much gentler (from −0.4 to −1.3 MPa/K) [7,8]. Therefore, other factors must account for significant depth variations of the 660-km discontinuity. In the present study, we presented the phase relations in anhydrous CMFAS-pyrolite to examine the influence of additional components and Mg/Si-ratio on PST and show that in the pyrolite system it occurs at nearly the same condition as it is observed in Mg_2SiO_4.

We have carried out several in situ X-ray diffraction experiments on decomposition of Rw to Mpv+Fpc and backward transformation and confirmed that PST can be expressed as P (GPa)=−0.0005 T (K)+23.54 using the Au EOS by Tsuchiya [20]. The transitional interval for coexistence of Rw and Mpv was found to be 0.1–0.5 GPa. The discrepancy between our data and the depth of the seismic discontinuity (global average 654 km) appears to be 20 km at 1850 K.

Based on the results of in situ observations we confirmed that the difference in chemical composition between pyrolite and Mg_2SiO_4 does not increase the negative Clapeyron slope of PST and most likely it varies between −0.4 and −1.3 MPa/K. Assuming the average mantle temperature 1850 K at 660 km we can account for only a half of variations in a depth of the 660-km discontinuity in subduction zones and hot spots using experimental data. Therefore, additional explanation for observed seismological variations at the 660 km (+20 and −50 km), which can involve influence of minor components or volatiles, is needed.

Acknowledgements

We thank D. Andrault, K. Collerson, T. Kondo, H. Terasaki and an anonymous reviewer for discussion and critical comments and S. Kato, T. Kawazoe, K. Tsuno, and R. Ando for technical help during experiments in SPring-8. KL thanks the Japan Society for Promotion of Sciences (JSPS) and 21st century COE program of Tohoku University for research fellowships. This work was supported by the grants in aid for Scientific Researches from Ministry of Education, Culture, Sports, Science and Technology, Japan (nos. 14102009 and 16075202) to E. Ohtani. This work was conducted as a part of the 21th COE program 'Advanced Science and Technology Center for the Dynamic Earth' at Tohoku University.

Appendix A

Table A1
Composition of the starting material (wt.%) used in present work compared with those used in the other high-pressure experiments in peridotite system

	SiO_2	TiO_2	Al_2O_3	Cr_2O_3	FeO	MgO	NiO	CaO	Na_2O	Total	Ref.
This work	45.3		4.42		8.20	38.2		3.86		100.0	
Pyrolite	45.0	0.20	4.45	0.40	8.05	37.8	0.25	3.55	0.36	99.8	[M]
Pyrolite	45.2	0.30	3.90	0.50	8.10	37.5	0.30	3.80	0.30	99.9	[I1, N]
KLB-1	44.5	0.16	3.59	0.31	8.10	39.2	0.25	3.44	0.30	100.0	[T, Z, H]
KR4003	44.9	0.16	4.26	0.41	8.02	37.3	0.24	3.45	0.22	99.1	[W1, I2]
MPY-90	45.1	0.17	3.88	0.45	7.61	38.9		3.41	0.50	100.0	[W2]

References:
MS—McDonough and Sun (1995) Chem. Geol., 120: 223–254.
I1—Irifune et al. [4] Science, 279: 1698–1700.
N—Nishiyama et al. [11] Phys. Earth Planet Inter., 143–144: 185–199.
T—Takahashi (1986) J. Geophys. Res, 91: 9367–9382.
Z—Zang and Herzberg (1994) J. Geophys. Res., 99: 17729–17742.
H—Hirose [10] J. Geophys. Res. 107, doi: 10.1029/2001JB000597.
W—Walter (1998) J. Petrol., 39: 29–60.
I2—Ito et al. (2004) Phys. Earth Planet. Inter., 143–144: 397–406.
W2—Wood [22] Earth Planet. Sci. Lett., 174: 341–354.

Table A2
Observed and calculated XRD lines of the sample Per-1-24 at 24.5 GPa and 1773 K

No.	d_{obs} (Å)	I/I_{100}	Mpv		Cpv		Fpc		Gt		Rw		
			d_{cal} (Å)	(hkl)	d_{cal} (Å)	(hkl)	d_{cal} (Å)	(hkl)	d_{cal} (Å)	(hkl)	d_{cal} (Å)	(hkl)	
1	3.3912	3	3.3902	(110)									
2	3.0314	2	3.0324	(111)									
3	2.8029	17							2.8043	(400)			
4	2.7942	18									2.7932	(220)	
5	2.5087	25							2.5082	(420)			
6	2.4904	11			2.4899	(110)							
7	2.4356	7	2.4357	(020)									
8	2.3986	52	2.3975	(112)									
9	2.3833	37									2.3820	(311)	
10	2.3603	16	2.3605	(200)									
11	2.3010	100											Au (111)
12	2.2005	8							2.1998	(431)			
13	2.1228	5	2.1243	(210)									
14	2.0641	42	2.0621	(121)			2.0645	(200)					
15	2.0393	29	2.0389	(103)									
16	2.0329	25			2.0330	(111)							
17	1.9928	32											Au (200)
18	1.9739	40									1.9751	(400)	
19	1.9395[a]	5											
20	1.8945	15											Au Kα2
21	1.8802	4	1.8809	(113)									
22	1.8485	16											Au Kα1
23	1.8215	8							1.8196	(611)			
24	1.8011	2	1.8002	(212)									
25	1.7601	8			1.7606	(200)							
26	1.6952	28	1.6955	(004)									
27	1.6126	4									1.6126	(422)	
28	1.5556	6							1.5555	(640)			
29	1.5188	22									1.5204	(511)	
30	1.4988	12	1.4979	(222)									
31	1.4607	8					1.4598	(220)					
32	1.4371	4			1.4375	(211)							
33	1.4092	11											Au (220)
34	1.3957	23	1.3988	(132)							1.3965	(440)	
35	1.3704	6	1.3699	(312)									
36	1.2453	3			1.2449	(220)							
37	1.2017	10											Au (311)
38	1.1915	3					1.1919	(222)					
39	1.1505	1											Au (222)

Unit-cell parameters are $a=4.721(2)$ Å, $b=4.871(2)$ Å, $c=6.782(3)$ Å, $V=155.97(9)$ Å^3 for Mg–perovskite (Mpv); $a=3.521(1)$ Å, $V=43.66(1)$ Å^3 for Ca–perovskite (Cpv); $a=4.129(1)$ Å, $V=70.39(6)$ Å^3 for ferropericlase (Fpc); $a=11.217(2)$ Å, $V=1411.3(9)$ Å^3 for majorite garnet (Gt); and $a=7.900(2)$ Å, $V=493.08(37)$ Å^3 for ringwoodite (Rw). Au, gold.

[a] Unidentified diffraction line.

Table A3
Observed and calculated XRD lines of the sample Per-2 at ambient conditions after the experiment

No.	d_{obs} (Å)	I/I_o	Mpv		Fpc		Gt		Rw		
			d_{cal} (Å)	(hkl)	d_{cal} (Å)	(hkl)	d_{cal} (Å)	(hkl)	d_{cal} (Å)	(hkl)	
1	3.4393	2	3.4405	(110)							
2	3.0836	3	3.0813	(111)							
3	2.8847	9					2.8858	(400)	2.8852	(220)	
4	2.5811	24					2.5811	(420)			
5	2.4692	12	2.4692	(020)							
6	2.4605	13							2.4605	(311)	
7	2.4432	21			2.4431	(111)					
8	2.4422	97	2.4408	(112)							
9	2.3989	5	2.3980	(200)							
10	2.3503	100									Au (111)
11	2.2635	6					2.2638	(431)			
12	2.1950	2	2.1953	(120)							
13	2.1564	2	2.1571	(210)							
14	2.1159	44			2.1158	(200)					
15	2.0791	8	2.0803	(103)							
16	2.0586	9	2.0596	(211)							
17	2.0346	31									Au (200)
18	1.9715	2	1.9715	(202)							
19	1.9390[a]	3									
20	1.9161	7	1.9172	(113)							
21	1.8983	9									Au Kα2
22	1.8722	7					1.8725	(611)	1.8722	(331)	
23	1.8538	1	1.8542	(122)							
24	1.8493	11									Au Kα1
25	1.7317	24	1.7317	(004)							
26	1.7213	28	1.7203	(220)							
27	1.6882	3	1.6865	(023)							
28	1.6667	7					1.6661	(444)	1.6658	(422)	
29	1.6015	4					1.6007	(640)			
30	1.5698	2							1.5705	(511)	
31	1.5422	4					1.5425	(642)			
32	1.5193	1	1.5191	(131)							
33	1.4946	14			1.4961	(220)					
34	1.4426	4							1.4426	(440)	
35	1.4380	12									Au (220)
36	1.4205	3	1.4201	(132)							
37	1.4043	2	1.4039	(204)							
38	1.3913	7	1.3926	(312)							
39	1.2913	2					1.2906	(840)			
40	1.2609	2					1.2595	(842)			
41	1.2250	17									Au (311)
42	1.2219	9			1.2216	(222)					
43	1.1756	1									Au (222)

Unit-cell parameters are $a=4.796(1)$ Å, $b=4.938(1)$ Å, $c=6.927(2)$ Å, $V=164.05(6)$ Å^3 for Mg–perovskite (Mpv); $a=4.232(1)$ Å, $V=75.77(2)$ Å^3 for ferropericlase (Fpc); $a=11.543(2)$ Å, $V=1538.1(6)$ Å^3 for majorite garnet (Gt); and $a=8.161(1)$ Å, $V=543.45(24)$ Å^3 for ringwoodite (Rw). Au, gold.

[a] Unidentified diffraction line.

References

[1] E. Ito, H. Yamada, Stability relations of silicate spinels, ilmenites, and perovskites, in: S. Akimoto, M.H. Manghnani (Eds.), High Pressure Research in Geophysics, Center for Academic Publications, Tokyo, Japan, 1982, pp. 27–48.

[2] E. Ito, E. Takahashi, Post-spinel transformation in the system Mg_2SiO_4–Fe_2SiO_4 and some geophysical implications, J. Geophys. Res. 94 (1989) 10637–10646.

[3] M. Akaogi, E. Ito, Refinement of enthalpy measurement of $MgSiO_3$ perovskite and negative pressure–temperature slopes for perovskite-forming reactions, Geophys. Res. Lett. 20 (1993) 1839–1842.

[4] T. Irifune, N. Nishiyama, K. Kuroda, T. Inoue, M. Isshiki, W. Utsumi, K. Funakoshi, S. Urakawa, T. Uchida, T. Katsura, O. Ohtaka, The postspinel phase boundary in Mg_2SiO_4 determined by in situ X-ray diffraction, Science 279 (1998) 1698–1700.

[5] L. Chudinovskikh, R. Boehler, High-pressure polymorphs of olivine and the 660-km seismic discontinuity, Nature 411 (2001) 574–577.

[6] S.H. Shim, T.S. Duffy, G. Shen, The post-spinel transformation in Mg_2SiO_4 and its relation to the 660-km seismic discontinuity, Nature 411 (2001) 571–574.

[7] T. Katsura, H. Yamada, T. Shinmei, A. Kubo, S. Ono, M. Kanzaki, A. Yoneda, M.J. Walter, E. Ito, S. Urakawa, K. Funakoshi, W. Utsumi, Post-spinel transition in Mg_2SiO_4 determined by high *P–T* in situ X-ray diffraction, Phys. Earth Planet. Inter. 136 (2003) 11–24.

[8] Y. Fei, J. Van Orman, J. Li, W. van Westrenen, C. Sanloup, W. Minarik, K. Hirose, T. Komabayashi, M. Walter, K. Funakoshi, Experimentally determined postspinel transformation boundary in Mg_2SiO_4 using MgO as an internal pressure standard and its geophysical implications, J. Geophys. Res. 109 (2004), doi:10.1029/2003JB002562.

[9] T. Irifune, A.E. Ringwood, Phase transformation in primitive MORB and pyrolite compositions to 25 GPa and some geophysical implications, in: M.H. Manghnani, Y. Syono (Eds.), High Pressure Research in Mineral Physics, Terra Pub., Tokyo, AGU, Washington DC, 1987, pp. 231–242.

[10] K. Hirose, Phase transition in pyrolitic mantle around 670-km depth: implications for upwelling of plumes from the lower mantle, J. Geophys. Res. 107 (2002), doi:10.1029/2001JB000597.

[11] N. Nishiyama, T. Irifune, T. Inoue, J. Ando, K. Funakoshi, Precise determination of phase relations in pyrolite across the 660 km seismic discontinuity by in situ X-ray diffraction and quench experiments, Phys. Earth Planet. Inter. 143–144 (2004) 185–199.

[12] O.L. Anderson, D.G. Issak, S. Yamamoto, Anharmonicity and the equation of state for gold, J. Appl. Phys. 65 (1989) 1534–1543.

[13] S. Speziale, C.-S. Zha, T.S. Duffy, R.J. Hemley, H.-K. Mao, Quasi-hydrostatic compression of magnesium oxide to 52 GPa: implications for the pressure–volume–temperature equation of state, J. Geophys. Res. 106 (2001) 515–528.

[14] M.P. Flanagan, P.M. Shearer, Global mapping of topography on transition zone velocity discontinuities by stacking SS precursors, J. Geophys. Res. 103 (1998) 2673–2692.

[15] J.D. Collier, G.R. Helffrich, B.J. Wood, Seismic discontinuities and subduction zones, Phys. Earth Planet. Inter. 127 (2001) 35–49.

[16] Y.J. Gu, A.M. Dziewonski, Global variability of transition zone thickness, J. Geophys. Res. 107 (2002), doi:10.1029/2001JB000489.

[17] C.R. Bina, G.R. Helffrich, Phase transition Clapeyron slopes and transition zone seismic discontinuity topography, J. Geophys. Res. 99 (1994) 15853–15860.

[18] M. Matsui, S.C. Parker, M. Leslie, The MD simulation of the equation of state of MgO: application as a pressure calibration standard at high temperature and high pressure, Am. Mineral. 85 (2000) 312–316.

[19] T. Kubo, E. Ohtani, T. Kato, S. Urakawa, A. Suzuki, Y. Kanbe, K. Funakoshi, W. Utsumi, T. Kikegawa, K. Fujino, Mechanism and kinetics of the post-spinel transformation in Mg_2SiO_4, Phys. Earth Planet. Inter. 129 (2002) 153–171.

[20] T. Tsuchiya, First-principles prediction of the *P–V–T* equation of state of gold and the 660-km discontinuity in Earth's mantle, J. Geophys. Res. 108 (2003), doi:10.1029/2003JB002446.

[21] Y. Fei, J. Li, K. Hirose, W. Minarik, J. Van Orman, C. Sanloup, W. van Westrenen, T. Komabayashi, K. Funakoshi, A critical evaluation of pressure scales at high temperatures by in situ X-ray diffraction measurements, Phys. Earth Planet. Inter. 143–144 (2004) 515–526.

[22] B.J. Wood, Phase transformations and partitioning relations in peridotite under lower mantle conditions, Earth Planet. Sci. Lett. 174 (2000) 341–354.

[23] N. Nishiyama, T. Yagi, Phase relation and mineral chemistry in pyrolite to 2200 °C under the lower mantle pressures and implications for dynamics of mantle plumes, J. Geophys. Res. 108 (2003), doi:10.1029/2002JB002216.

[24] D. Frost, F. Langenhorst, The effect of Al_2O_3 on Fe–Mg partitioning between magnesiowüstite and magnesium silicate perovskite, Earth Planet. Sci. Lett. 199 (2002) 227–241.

[25] J.C. Jamieson, J.N. Fritz, M.H. Manghnani, Pressure measurement at high temperature in X-ray diffraction studies: gold as a primary standard, in: S. Akimoto, M.H. Manghnani (Eds.), High Pressure Research in Geophysics, Center for Academic Publications, Tokyo, Japan, 1982, pp. 27–48.

[26] S.-H. Shim, T.S. Duffy, K. Takemura, Equation of state of gold and its application to the phase boundaries near 660 km depth in Earth's mantle, Earth Planet. Sci. Lett. 203 (2002) 729–739.

[27] M. Matsui, N. Shima, Electronic thermal pressure and equation of state of gold at high temperature and high pressure, J. Appl. Phys. 93 (2003) 9679–9682.

[28] M. Okube, A. Yoshiasa, O. Ohtaka, H. Fukui, Y. Katayama, W. Utusmi, Anharmonic effective pair potentials of gold under high pressure and high temperature, J. Phys., Condens. Matter 14 (2002) 11511–11515.

[29] M. Akaogi, E. Ito, A. Navrotsky, Olivine-modified spinel–spinel transitions in the system Mg_2SiO_4–Fe_2SiO_4: calorimetric measurements, thermochemical calculation, and geophysical application, J. Geophys. Res. 94 (1989) 15671–15685.

[30] J. Li, C. Hadidiacos, H.K. Mao, Y. Fei, R.J. Hemley, Behavior of thermocouples under high pressure in a multi-anvil apparatus, High Press. Res. 23 (2003) 389–401.
[31] H.K. Mao, J. Xu, P.M. Bell, Calibration of the ruby pressure gauge to 800 kbar under quasi-hydrostatic conditions, J. Geophys. Res. 91 (1986) 4673–4676.
[32] S.H. Kirby, S. Stein, E.A. Okal, D.C. Rubie, Metastable mantle phase transformations and deep earthquakes in subducting oceanic lithosphere, Rev. Geophys. 34 (1996) 261–306.
[33] Y. Fei, J. Van Orman, W. van Westrenen, J. Li, C. Sanloup, T. Komabayashi, K. Funakoshi, In situ X-ray diffraction measurements of the postspinel transition in a peridotitic composition, EOS Trans. AGU 83 (47) (2002) F977.
[34] Y.J. Gu, A.M. Dziewonski, G. Ekström, Simultaneous inversion for mantle shear velocity and topography of transition zone discontinuities, Geophys. J. Int. 154 (2003) 559–583.
[35] D.L. Anderson, J.D. Bass, Transition region of the Earth's upper mantle, Nature 320 (1986) 321–328.
[36] S. Lebedev, S. Chevrot, R.D. van der Hilst, Correlation between the shear-speed structure and thickness of the mantle transition zone, Phys. Earth Planet. Inter. 136 (2003) 25–40.
[37] F. Niu, H. Kawakatsu, Direct evidence for the undulation of the 660-km discontinuity beneath Tonga: comparison of Japan and California array data, Geophys. Res. Lett. 22 (1995) 531–534.
[38] C.W. Wick, M.A. Richards, A detailed map of the 660-kilometer discontinuity beneath the Izu-Bonin subduction zone, Science 261 (1993) 1424–1427.
[39] J.C. Castle, K.C. Creager, Topography of the 660-km seismic discontinuity beneath Izu-Bonin: implications for tectonic history and slab deformation, J. Geophys. Res. 103 (1998) 12511–12527.
[40] J.E. Vidale, H.M. Benz, Upper-mantle seismic discontinuities and the thermal structure of subduction zones, Nature 356 (1992) 678–683.
[41] Y. Shen, S.C. Solomon, I.T. Bjarnason, C.J. Wolfe, Seismic evidence for a lower-mantle origin of the Iceland plume, Nature 395 (1998) 62–65.
[42] X. Li, R. Kind, K. Priestley, S.V. Sobolev, F. Tilmann, X. Yuan, M. Weber, Mapping the Hawaiian plume conduit with converted seismic waves, Nature 405 (2000) 938–941.
[43] F. Niu, H. Inoue, D. Suegetsu, K. Kanjo, Seismic evidence for a thinner mantle transition zone beneath the South Pacific superswell, Geophys. Res. Lett. 27 (2000) 1981–1984.
[44] T. Murakami, S. Yoshioka, The relationship between the physical properties of the assumed pyrolite composition and depth distributions of seismic velocities in the upper mantle, Phys. Earth Planet. Inter. 125 (2001) 1–17.
[45] M. Akaogi, A. Tanaka, E. Ito, Garnet–ilmenite–perovskite transitions in the system $Mg_4Si_4O_{12}$–$Mg_3Al_2Si_3O_{12}$ at high pressures and high temperatures: phase equilibria, calorimetry and implications for mantle structure, Phys. Earth Planet. Inter. 132 (2002) 303–324.
[46] K.D. Litasov, E. Ohtani, Phase relations in hydrous MORB at 18–28 GPa: implications for heterogeneity of the lower mantle, Phys. Earth Planet. Inter. 150 (2005) 239–263.
[47] A.M. Dziewonski, D.L. Anderson, Preliminary reference Earth model, Phys. Earth Planet. Inter. 25 (1981) 297–356.
[48] B.L.N. Kennet, E.R. Engdahl, R. Buland, Constrains on seismic velocities in the Earth from traveltimes, Geophys. J. Int. 122 (1995) 108–124.
[49] I. Jackson, Elasticity, composition and temperature of the Earth's lower mantle: a reappraisal, Geophys. J. Int. 134 (1998) 291–311.
[50] F. Deschamps, J. Trampert, Towards a lower mantle reference temperature and composition, Earth Planet. Sci. Lett. 222 (2004) 161–175.
[51] W.M. Kaula, Minimal upper mantle temperature variations consistent with observed heat flow and plate velocities, J. Geophys. Res. 88 (1983) 10323–10332.
[52] E. Ohtani, K. Litasov, T. Hosoya, T. Kubo, T. Kondo, Water transport into the deep mantle and formation of a hydrous transition zone, Phys. Earth Planet. Inter. 143–144 (2004) 255–269.
[53] A.M. Hoffmeister, Mantle values of thermal conductivity and the geotherm from phonon lifetimes, Science 283 (1999) 1699–1706.
[54] C. Herzberg, P. Raterron, J. Zhang, New experimental observations on the anhydrous solidus for peridotite KLB-1, Geochem. Geophys. Geosyst. 1 (2000), doi:10.1029/2000GC000089.
[55] D.L. Kohlstedt, H. Keppler, D.C. Rubie, Solubility of water in the α, β, and γ phases of $(Mg, Fe)_2SiO_4$, Contrib. Mineral. Petrol. 123 (1996) 345–357.
[56] N. Bolfan-Casanova, S. Mackwell, H. Keppler, C. McCammon, D. Rubie, Pressure dependence of H solubility in magnesiowüstite up to 25 GPa: implications for the storage of water in the Earth's lower mantle, Geophys. Res. Lett. 29 (2002), doi:10.1029/2001GL014457.
[57] N. Bolfan-Casanova, H. Keppler, D.C. Rubie, Water partitioning at 660 km depth and evidence for very low water solubility in magnesium silicate perovskite, Geophys. Res. Lett. 30 (2003), doi:10.1029/2003GL017182.
[58] Y. Higo, T. Inoue, T. Irifune, H. Yurimoto, Effect of water on the spinel–postspinel transformation in Mg_2SiO_4, Geophys. Res. Lett. 28 (2001) 3505–3508.
[59] K.D. Litasov, E. Ohtani, A. Sano, A. Suzuki, K. Funakoshi, Wet subduction versus cold subduction, Geophys. Res. Lett. 32 (2005) L13312, doi:10.1029/2005GL022921.
[60] H.M. Benz, J.E. Vidale, Sharpness of upper-mantle discontinuities determined from high-frequency reflections, Nature 365 (1993) 147–150.
[61] L. Stixrude, Structure and sharpness of phase transitions and mantle discontinuities, J. Geophys. Res. 102 (1997) 14835–14852.